

WORDT
NIET UITGELEEND

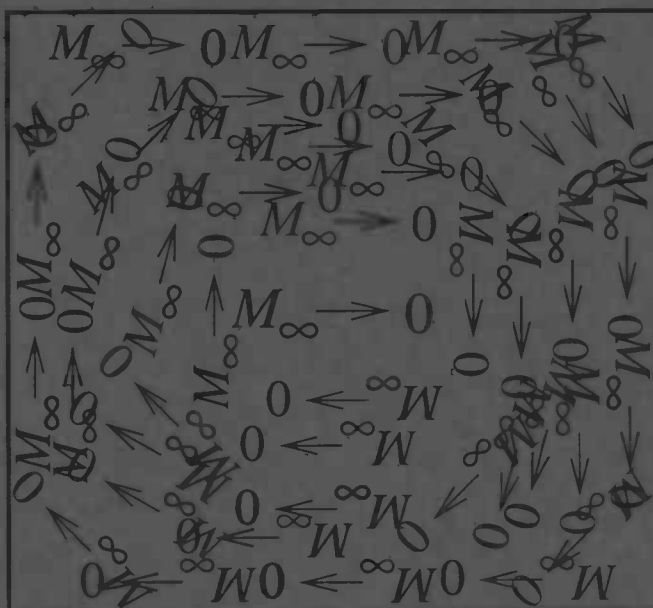


Solving the Navier-Stokes Equations at Low Mach Numbers

Ronald Rook

Rijksuniversiteit Groningen
Bibliotheek
Wiskunde / Informatica / Rekencentrum
Landelven 5
Postbus 800
9700 AV Groningen

29 NOV 1990



Department of
Mathematics

RuG



Master's thesis

Solving the Navier-Stokes Equations at Low Mach Numbers

Ronald Rook

University of Groningen
Department of Mathematics
P.O. Box 800
9700 AV Groningen

29 NOV. 1996

November 1996

Contents

1	Introduction	3
2	The Navier-Stokes equations	5
2.1	The differential equations	5
2.2	The thermodynamical relations	5
2.3	The test problem	6
2.4	Scaling	6
2.5	Boundary conditions	9
3	Discretization in space	11
3.1	Staggered grid	11
3.2	The finite difference method	11
4	Stability and Convergence	15
4.1	Well-posed initial-value problems	16
4.2	Stability	17
5	Implementation	19
5.1	Newton's method	19
5.2	The preconditioner	20
6	Results	23
6.1	Reynolds number and artificial diffusion	23
6.2	Time propagation to steady state	23
6.3	Time step	24
6.4	Indefiniteness of the density	24
6.5	The zero Mach limit	26
6.6	Scaling performance	28
7	Mass conservation	33
8	Pushing the method to its limits	37
9	Concluding remarks	41

Rijksuniversiteit Groningen
Bibliotheek
Wiskunde / Informatica / Rekencentrum
Landleven 5
Postbus 800
9700 AV Groningen

[The following text is extremely faint and illegible, appearing to be a list or series of entries.]

2
Gardner

Chapter 1

Introduction

When we talk about the investigation of numerical methods for the different types of flows, we may divide that area in compressible and incompressible flows. Both flows are described by the Navier-Stokes equation. For compressible flows we need an additional equation, the equation of state, which couples the pressure to the density. In order to connect these different areas we introduce the Mach number, which is the quotient of the velocity and the speed of sound. When, after a proper scaling, the Mach number is taken zero we have the incompressible equations. The question is whether the solutions of those also converge when Mach number tends to zero. Investigators try to develop methods that handle the equations their characteristic behavior: References [1, 2] and others mentioned several problems in calculating low Mach number flows. The first one is the stiffness of the governing equations. Since the eigenvalues correspond to the speeds of the waves carrying information, one class of information will hardly be transported anywhere for $M \rightarrow 0$ in an explicit calculation. In these methods the time step is limited by the fastest travelling wave. The number of time steps needed to establish a steady state will tend to infinity in the compressible limit. A way to overcome the stiffness is the use of implicit schemes involving preconditioning the to be inverted Jacobian matrix.

The second problem is the fact that certain flow quantities become singular as Mach number tends to zero. This should be avoided by careful scaling. We will use one quite similar to that used in [3] where the so-called pressure coefficient $C_p = 2(p - 1/\gamma M_0^2)$ is defined. When we substitute it in the Navier-Stokes equations the diverging constant term will vanish from the pressure gradient. Reference [1] proposed also a scaled temperature of the same kind based on the Eckert number: $\tilde{T} = 1/Ec = c_p T/u_0 - 1/(\gamma - 1)M_0^2$. With u_0 and M_0 respectively a reference velocity and a reference Mach number. In [4] the same scaling is used and one can find the resulting dimensionless equation, but it is not a low-Mach number formulation: the incompressible equations are not recovered from them.

This shows another gap concerning what primary variables we have to use. Most compressible codes have the conservative variables $\rho, \rho u, \rho v$ and ρE as primary

variables, whereas the primitive variables u, v, p and T are used in the pressure-based incompressible codes. To close the gap we have to make a choice. The choice will be the latter one. Firstly in this case the incompressible equations are *directly* derived from the compressible ones when the Mach number is taken zero. For example the question whether the velocity field is divergence free in an incompressible flow becomes a trivial one in this case. That is also an advantage of having the primitive variables available.

The test-problem that we use to investigate the behavior of the solution is the square-driven cavity. This is a widely used configuration in incompressible flow simulations. Many reference material is available [5, 6, 7] for the validation of solutions. We will make use of a staggered equidistant grid, which is not very common in the compressible world. Reference [8] reported the use of such a grid, though. What we will investigate is especially the behavior of the pressure, and the, via the equation of state related, density.

Having a code producing solutions at arbitrary Mach numbers, we would like to investigate the convergence of the solutions of the compressible equations to those of the incompressible ones. If this turns out to be successful we have a closure for the gap between the two worlds: a unified method for both cases.

In most cases of developing such a method it is an extension of an existing code. In our case we start from a fully implicit steady-state incompressible flow solver: it simultaneously solves all equations. This is to be favored to the common pressure correction methods in which velocities and pressures are computed alternately (e.g. SIMPLE, PISO, ADI [9]).

Chapter 2

The Navier-Stokes equations

2.1 The differential equations

The Navier-Stokes equations are a set of coupled partial differential equations, describing the time evolution of fluids. The equations read:

$$\begin{aligned} \frac{D\rho}{Dt} + \rho(u_x + v_y) &= 0 & (2.1) \\ \rho \frac{Du}{Dt} + p_x - \left(\frac{4}{3}(\mu u_x)_x + (\mu u_y)_y - \frac{2}{3}(\mu v_y)_x + (\mu v_x)_y\right) &= 0 \\ \rho \frac{Dv}{Dt} + p_y - \left(\frac{4}{3}(\mu v_y)_y + (\mu v_x)_x - \frac{2}{3}(\mu u_x)_y + (\mu u_y)_x\right) &= 0 \\ \rho \frac{De}{Dt} - \frac{p}{\rho} \frac{D\rho}{Dt} - \mu(2(u_x^2 + v_y^2) - \frac{2}{3}(u_x + v_y)^2 + (u_y + v_x)^2) \\ &- (kT_x)_x - (kT_y)_y = 0 \end{aligned}$$

Where $\frac{D}{Dt}$ denotes the total derivative and where ρ represents the density, p the pressure, T the temperature, u, v the velocity components and e the internal energy in the system. μ represents the dynamical viscosity.

2.2 The thermodynamical relations

In an ideal gas we have the following relations between the quantities in the Navier-Stokes equations. The symbols c_p and c_v denote the heat capacity at constant pressure and constant volume respectively; Pr the Prandtl number and a the speed of sound.

$$\begin{aligned} p &= \rho RT, & e &= c_v T, & a^2 &= \gamma p / \rho, \\ \gamma &= c_p / c_v, & R &= c_p - c_v, & Pr &= c_p \mu / k \end{aligned}$$

The values of γ and Pr are taken to be 1.4 and 0.72 respectively.

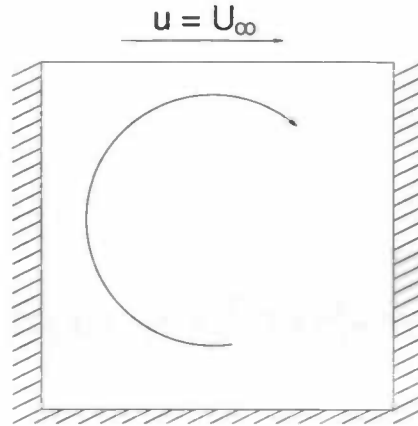


Figure 2.1: The driven cavity

2.3 The test problem

As a test problem the square driven cavity with an impulsively started lid is taken as shown in figure 2.1. This configuration is defined by a rectangular region $\Omega = [0, l] \times [0, l] \subset \mathbb{R}^2$. Boundary conditions are $T = T_\infty$ and $u = v = 0$ at $\partial\Omega$, except at the edge $y = l$, where $u = U_\infty$ is taken. For the initial condition we take

$$\rho = \rho_\infty, \quad T = T_\infty, \quad p = p_\infty, \quad u = 0, \quad v = 0$$

2.4 Scaling

The next step is to find proper scaling values. For the driven cavity problem, there are a reference length, velocity, density, pressure and temperature: l , U_∞ , ρ_∞ , p_∞ and T_∞ . The values U_r , ρ_r , p_r and T_r , we will use for non-dimensionalizing the quantities, remain to be chosen. We scale the independent quantities on a natural way. If we non-dimensionalize the other quantities with its reference values satisfying the gas law $p_\infty = \rho_\infty R T_\infty$ it gives rise to a singular system of equation when the reference Mach number $M_\infty = u_\infty/a_\infty$ is taken zero. For instance the x -impulse equation will be:

$$\rho \frac{Du}{Dt} + \frac{p_\infty}{\rho_\infty u_\infty^2} \frac{\partial p}{\partial x} + \dots = 0 \quad (2.2)$$

We may rewrite this to

$$\rho \frac{Du}{Dt} + \frac{1}{\gamma M_\infty^2} \frac{\partial p}{\partial x} + \dots = 0 \quad (2.3)$$

We see that for small Mach numbers the terms are not of the same order and that the system is even singular when Mach number is taken zero. Therefore we need

a new formulation.

If we interpret the Mach number limit as the limit of the velocity of the lid to zero with a constant reference speed of sound a_∞ we see that

$$p \rightarrow p_\infty, \quad T \rightarrow T_\infty, \quad \rho \rightarrow \rho_\infty \quad \text{and} \quad u, v \rightarrow 0 \quad (2.4)$$

In order to avoid loss of accuracy we first subtract those constants before non-dimensionalizing. A common way to non-dimensionalize the pressure is dividing it by $\rho_\infty u_\infty^2$, which is twice the dynamical reference pressure, so we have all terms in the x -impulse equation of same order. Thus in general we are looking for the scalings:

$$\tilde{p} = \frac{p - p_c}{p_r}, \quad \tilde{\rho} = \frac{\rho - \rho_c}{T_r}, \quad \tilde{T} = \frac{T - T_c}{T_r}, \quad \tilde{u} = \frac{u - u_c}{u_r}, \quad \tilde{v} = \frac{v - v_c}{u_r}, \quad (2.5)$$

In order to find the scaling factors with subscript r , we consider the flow as a thermodynamical equilibrium with a constant entropy along streamlines, which is just a rough indication of the solution. If the entropy is defined as

$$DS = c_p D(\ln T) - RD(\ln p) = c_v D(\ln T) - RD(\ln \rho) \quad (2.6)$$

we can derive that

$$\frac{c_v}{T_\infty}(T - T_\infty) - \frac{R}{p_\infty}(p - p_\infty) \approx 0 \quad (2.7)$$

by integrating along a path near the region with the constant flow properties. We already have scaled the pressure as in (2.5) so we can derive that

$$\frac{T - T_\infty}{T_\infty} \sim \tilde{p} \frac{p_r}{p_\infty} \quad \text{and} \quad \frac{\rho - \rho_\infty}{\rho_\infty} \sim \tilde{\rho} \frac{p_r}{p_\infty} \quad (2.8)$$

Choosing $p_r = \rho_\infty u_\infty^2$ we can derive, using the equations of state, the following scaled quantities

$$\tilde{\rho} = \frac{\rho - \rho_\infty}{\gamma M_\infty^2 \rho_\infty}, \quad \tilde{T} = \frac{T - T_\infty}{\gamma M_\infty^2 T_\infty}, \quad \tilde{p} = \frac{p - p_\infty}{\gamma M_\infty^2 p_\infty} \quad (2.9)$$

Of course we take $u_r = U_\infty$, since the moving lid determines eventually the velocity in the cavity. For the complete picture the other dimensionless quantities are

$$\tilde{u} = \frac{u}{U_\infty}, \quad \tilde{v} = \frac{v}{U_\infty}, \quad \tilde{t} = \frac{t}{t_0}, \quad \tilde{x} = \frac{x}{l}, \quad \tilde{y} = \frac{y}{l}, \quad \tilde{\mu} = \frac{\mu}{\mu_\infty} \quad (2.10)$$

with $t_0 = l/U_\infty$. Those dimensional quantities result in a system of partial differential equations in the unknowns $\tilde{\rho}$, \tilde{p} , \tilde{T} , \tilde{u} and \tilde{v} . The dimensionless equations are:

$$\gamma M_\infty^2 \frac{D\rho}{Dt} + (\gamma M_\infty^2 \rho + 1)(u_x + v_y) = 0 \quad (2.11)$$

$$\begin{aligned}
(\gamma M_\infty^2 \rho + 1) \frac{Du}{Dt} + p_x - \frac{1}{Re} \left(\frac{4}{3} (\mu u_x)_x + (\mu u_y)_y - \frac{2}{3} (\mu v_y)_x + (\mu v_x)_y \right) &= 0 \\
(\gamma M_\infty^2 \rho + 1) \frac{Dv}{Dt} + p_y - \frac{1}{Re} \left(\frac{4}{3} (\mu v_y)_y + (\mu v_x)_x - \frac{2}{3} (\mu u_x)_y + (\mu u_y)_x \right) &= 0 \\
(\gamma M_\infty^2 \rho + 1) \frac{DT}{Dt} - \frac{\gamma - 1}{\gamma} \left(\frac{Dp}{Dt} + \frac{\mu}{Re} \mathcal{D} \right) - \frac{1}{Re Pr} \left((\mu T_x)_x + (\mu T_y)_y \right) &= 0 \\
p = \gamma M_\infty^2 \rho T + \rho + T & \tag{2.12}
\end{aligned}$$

where

$$\mathcal{D} = 2(u_x^2 + v_y^2) - \frac{2}{3}(u_x + v_y)^2 + (u_y + v_x)^2$$

and the parameters Re has been introduced

$$Re = \frac{\rho_\infty U_\infty l}{\mu_\infty}$$

called Reynolds number

Note when the Mach number is taken zero, the first three equations become the familiar incompressible Navier-Stokes equations. In that case the pressure and the velocity are derived from the first three equations. Also when γ is taken 1 the energy equation becomes a pure convection-diffusion equation for the temperature. We see, when the Mach number is zero, that the pressure level is not fixed. In that case the density is not fixed as well and the term $\frac{Dp}{Dt}$ in the energy equation becomes erroneous. We will show the fixation of the level of p for $M_\infty = 0$ for the cavity. If we define total mass as

$$\int_{\Omega} \rho dV$$

we see it may leak: conservation of mass will not be described by the equations anymore. For Mach number not equal to zero the continuity equation can be written in its conservative form. If Ω denotes the flow region, we have

$$\gamma M_\infty^2 \int_{\Omega} \frac{\partial}{\partial t} \rho dV + \int_{\Omega} \text{div}(\gamma M_\infty^2 \rho + 1) \mathbf{u} dV = 0 \tag{2.13}$$

or

$$\gamma M_\infty^2 \frac{d}{dt} \int_{\Omega} \rho dV + \int_{\partial\Omega} (\gamma M_\infty^2 \rho + 1) \mathbf{u} \cdot \mathbf{n} dS = 0 \tag{2.14}$$

and since we have neither in- nor outflow at the boundary we simply have $\frac{d}{dt} \int \rho dV = 0$. Hence, for arbitrary non-zero Mach number we have mass conservation. But in our formulation the term vanishes when the Mach number is taken zero. We

now simply require the mass conservation in this limit case. Thus for the cavity we add the equation

$$\int \rho dV = 0 \quad (2.15)$$

This fixes the level of the density and the pressure at $M_\infty = 0$. It makes it possible to compute the solution for small M_∞ from the $M_\infty = 0$ case.

We have derived that the condition is also consistent with the equations when Mach number is not zero. We then may omit this equation. In the Chapter 7 we will see it is numerically a stronger condition than the equations themselves due to roundoff errors. In that regard it will be handy to have an overdetermined (but non-conflicting) system to solve.

Finally, the temperature dependence of μ is specified as

$$\mu = (\gamma M_\infty^2 T + 1)^{\frac{3}{2}} \frac{1 + \tilde{S}}{\gamma M_\infty^2 T + 1 + \tilde{S}} \quad (2.16)$$

as known as the Sutherland's law. \tilde{S} denotes the dimensionless quotient of a reference temperature and an effective temperature S called the Sutherland's constant, which is characteristic of the gas. This could be inserted as a parameter in the problem. For air we have $\tilde{S} = 0.4$ when the reference temperature is $273K$. We mention that the Sutherland's law may be replaced by a power law:

$$\mu = (\gamma M_\infty^2 T + 1)^n$$

with $n = 0.666$ for air, but is less accurate than (2.16). All numbers are from Reference [4].

2.5 Boundary conditions

In the flow we take the no-slip conditions on a wall which are

$$u = v = 0 \quad (2.17)$$

Further we assume that the boundary is of constant temperature. The scaled condition for \tilde{T} when $T = T_\infty$ on the edge is undetermined when Mach number is taken 0. But for arbitrary small Mach number the boundary condition \tilde{T} is zero, assuming continuity the boundary limit will also be zero, hence $T = 0$ at the boundary.

There are many things that we can do to help our country.

1. We can be good citizens.

2. We can help our neighbors. We can help them if they are in trouble. We can help them if they are sick. We can help them if they are poor. We can help them if they are old. We can help them if they are young. We can help them if they are disabled. We can help them if they are in need.

3. We can help our country.

4. We can help our world.

5. We can help our planet. We can help our planet by recycling. We can help our planet by saving water. We can help our planet by saving energy. We can help our planet by planting trees. We can help our planet by using public transportation.

6. We can help our future.

7. We can help our children.

8. We can help our country.

9. We can help our world.

10. We can help our planet.

11. We can help our future. We can help our future by being good citizens. We can help our future by helping our neighbors. We can help our future by helping our country. We can help our future by helping our world. We can help our future by helping our planet. We can help our future by helping our children.

Chapter 3

Discretization in space

3.1 Staggered grid

For the discretization in space we use a equidistant staggered grid, where the density, pressure and temperature are defined in the center and the velocity at the edges of a grid cell as shown in Figure 3.1. Such a staggered grid comes from the incompressible world and avoids the so-called decoupling of the pressure. We will employ it following Reference [8]. Although it is not customary in the compressible world where decoupling is mostly handled by artificial diffusion.

3.2 The finite difference method

Our discretization will be a finite difference one. If we consider the center cell in Figure 3.1, the momentum equations are evaluated in respectively the places where the velocity components u , v are defined. The energy and the continuity equation will be evaluated in the center. Because quantities are not defined in all places, the use of averages is needed. We now give a summary of the actions that will be done in different parts of our equations:

continuity equation Since mass conservation in a driven cavity is intuitively clear (see Section 2.4), we use the conservative form. We apply a central differencing scheme and achieve conservation of mass in the discrete formulation. The semi-discretization is as follows:

$$\begin{aligned} \gamma M_\infty^2 \frac{d}{dt} \rho_C &+ \frac{1}{h} [(\gamma M_\infty^2 \rho_O + 1)u_O - (\gamma M_\infty^2 \rho_W + 1)u_W] \\ &+ \frac{1}{k} [(\gamma M_\infty^2 \rho_N + 1)v_N - (\gamma M_\infty^2 \rho_Z + 1)v_Z] = 0 \end{aligned} \quad (3.1)$$

And indeed, if we calculate the total mass by summing the equations over all cells we have $\frac{d}{dt}(\text{total mass}) + (\text{mass flux through the edges}) = 0$ and since our problem

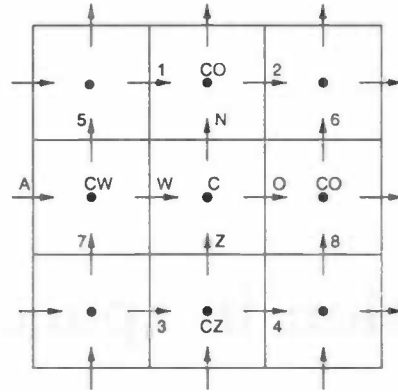


Figure 3.1: Placing the primaries

does not have inflow nor outflow boundaries, we achieve that our cavity does not leak in a numerical way, in an exact computation as long as $M_\infty \neq 0$.

convection For the convective part we use a first-order upwind differencing scheme. Let us consider a convective term $\rho u \frac{\partial u}{\partial x}$ which will be evaluated in point W . We get

$$(\gamma M_\infty^2 \rho_W + 1) u_W \frac{1}{h} \begin{cases} u_O - u_W & \text{if } u_W > 0 \\ u_W - u_A & \text{if } u_W < 0 \end{cases}$$

diffusion and pressure gradient The diffusive (or dissipative) part will be a second-order central one. Thus, a term like $\frac{\partial}{\partial x} (\mu \frac{\partial u}{\partial x})$ in point W will be

$$\frac{1}{h^2} [\mu_C (u_O - u_W) - \mu_{CW} (u_W - u_A)]$$

Also for the terms in the dissipation \mathcal{D} and the pressure gradient we use space-centered differences. A term like $\frac{\partial p}{\partial x}$ in point W will be

$$\frac{1}{h} [p_C - p_{CW}]$$

the gas law Since all quantities in the gas law are defined in the same point, therefore its discretization is simply $p_C = \gamma M_\infty^2 \rho_C T_C + \rho_C + T_C$

boundary treatment A few comments has to be made on treating boundary conditions. Firstly, a consequence of using a staggered grid is that boundary values are needed that do not directly correspond to the values in their grid points, so mirroring is necessary. If we look at a vertical moving wall as in Figure 3.2. The boundary condition $v = v_{\text{wall}}$ becomes $v_7 = 2v_{\text{wall}} - v_Z$. Secondly, in the energy equation a pressure gradient is needed at the wall. In the case that the velocity in

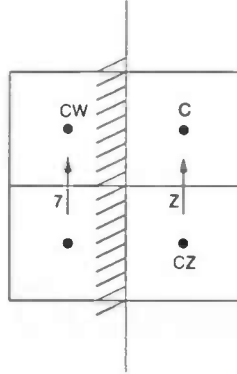


Figure 3.2: Mirroring the velocity

the center of a boundary cell has a direction away from our vertical wall we have a term $u \frac{\partial p}{\partial x}|_{\text{wall}}$. Since this component is of order $O(h)$ in the boundary cell, we may set it to zero.

We now can write the semi-discretization of the Navier-Stokes equations as:

$$(\gamma M_{\infty}^2 \rho_W + 1) \frac{d}{dt} u_W + F_2 = 0 \quad (3.2)$$

$$(\gamma M_{\infty}^2 \rho_Z + 1) \frac{d}{dt} v_Z + F_3 = 0$$

$$\gamma M_{\infty}^2 \frac{d}{dt} \rho_C + F_1 = 0$$

$$(\gamma M_{\infty}^2 \rho_C + 1) \frac{d}{dt} T_C - \frac{\gamma - 1}{\gamma} \frac{d}{dt} p + F_4 = 0 \quad (3.3)$$

$$\text{and } p_C = \gamma M_{\infty}^2 \rho_C T_C + \rho_C + T_C \quad (3.4)$$

where the F_i 's are the discretized versions of the stationary part of the equations.

Chapter 4

Stability and Convergence

A main property of a working method for solving a system is convergence. We would like to obtain the analytical solution for our problem. So all we need is a property telling that the global truncation-error will tend to zero by mesh-refinement. For the determination we now would like to use a theorem like Lax's Equivalence Theorem [10] to hand tools for a direct investigation of convergence. But the non-linearity of the equations and therefore the non-uniqueness of the solutions limit us there. Lax's theorem can only be applied to linear systems with a proper definition of stability. The way left is to approximate the non-linear equation with linear equation and hope it will have, at least *locally*, the same properties as the non-linear ones. By doing so we may say by the words of Lax's theorem that a well-posed initial value problem with a consistent difference scheme, stability is a necessary and sufficient condition for convergence.

Before we are able to do these investigation we need to linearize the equations. Here we assume a constant viscosity and linearize around a constant vector field: $\phi = \phi_c + \tilde{\phi}$. After we also eliminate the density in order to have the u, v, p, T -formulation, the equations will then read after dropping the tildes

$$\left(K \frac{\partial}{\partial t} + A\left(\frac{\partial}{\partial x}, \frac{\partial}{\partial y}\right)\right)\phi(x, y, t) = 0 \quad (4.1)$$

with

$$K = \begin{bmatrix} 1 & 0 & 0 & 0 \\ 0 & 1 & 0 & 0 \\ -\gamma M_\infty^2 & 0 & 0 & \gamma M_\infty^2 \\ -\frac{\gamma-1}{\gamma} & 0 & 0 & 1 \end{bmatrix} \quad (4.2)$$

$$A\left(\frac{\partial}{\partial x}, \frac{\partial}{\partial y}\right) = \quad (4.3)$$

$$\begin{bmatrix} \text{div} - \frac{1}{Re} \left(\frac{4}{3} \frac{\partial^2}{\partial x^2} + \frac{\partial^2}{\partial y^2} \right) & -\frac{1}{Re} \frac{1}{3} \frac{\partial^2}{\partial x \partial y} & \frac{\partial}{\partial x} & 0 \\ -\frac{1}{Re} \frac{1}{3} \frac{\partial^2}{\partial x \partial y} & \text{div} - \frac{1}{Re} \left(\frac{4}{3} \frac{\partial^2}{\partial y^2} + \frac{\partial^2}{\partial x^2} \right) & \frac{\partial}{\partial y} & 0 \\ \frac{\partial}{\partial x} & \frac{\partial}{\partial y} & \gamma M_\infty^2 \text{div} & -\gamma M_\infty^2 \text{div} \\ 0 & 0 & -\frac{\gamma-1}{\gamma} \text{div} & \text{div} - \frac{1}{Pr Re} \Delta \end{bmatrix}$$

and $\phi = \begin{bmatrix} u \\ v \\ p \\ T \end{bmatrix}, \quad \phi_c = \begin{bmatrix} 1 \\ 1 \\ 0 \\ 0 \end{bmatrix}$ (4.4)

A point that needs to be investigated is the behavior of the system in the limit $M_\infty \rightarrow 0$.

4.1 Well-posed initial-value problems

The first thing to investigate is whether a system of equations is well-posed: is the solution with initial value $\phi(x, y, 0) = \phi_0(x, y)$ bounded on a finite time interval? To answer that question we use its Fourier components to analyze the behavior of the solutions in time. When neglecting the influence of boundary conditions we may write the solution ϕ in terms of its Fourier components as

$$\phi(x, y, t) = \frac{1}{2\pi} \int \int \hat{\phi}(\zeta, \eta, t) e^{i(x\zeta + y\eta)} d\zeta d\eta \quad (4.5)$$

When we substitute this in (4.1) it yields

$$\left(K \frac{\partial}{\partial t} + A(i\zeta, i\eta) \right) \hat{\phi}(\zeta, \eta, t) = 0 \quad (4.6)$$

Suppose we may write the Fourier transformed solution as

$$\hat{\phi}(\zeta, \eta, t) = \sum_{j=1}^k \hat{w}_j(\zeta, \eta) e^{\lambda_j(\zeta, \eta)t} \quad (4.7)$$

with \hat{w}_j vector-valued eigenfunctions belonging to the eigenvalues λ_j from the generalized eigenvalue problem

$$(\lambda K + A) \hat{w} = 0 \quad (4.8)$$

then the solution is bounded on a finite interval if the real part of eigenvalues are located in the left half of the complex plane. Figure 4.1 shows the eigenvalues for the ζ -axis in the ζ, η -plane for $M_\infty^2 = 0.1$ and $Re = 100$. The four eigenvalues are the parabolic curves in picture. We now let M_∞ tend to zero and observe (Figure 4.2) that two eigenvalues are running away. Those are the outer curves in the figure. And if the Mach number is taken zero just two eigenvalues are left

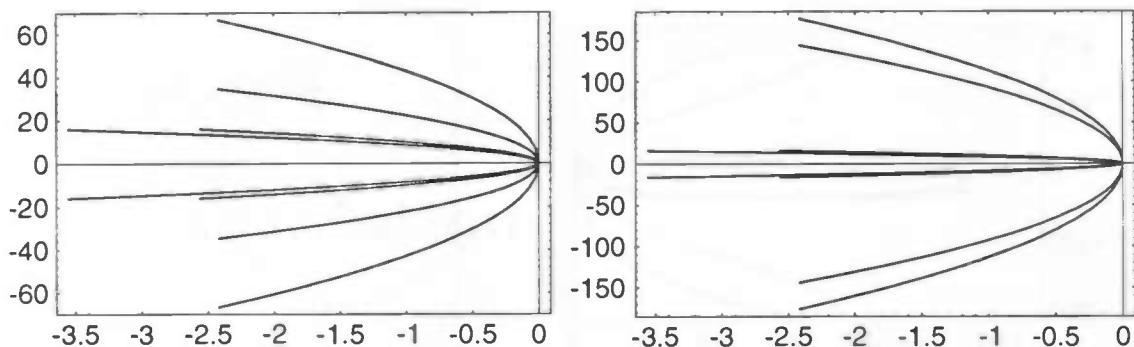


Figure 4.1: Eigenvalues at $M_\infty^2 = 0.1$ and $Re = 100$ at $\eta = 0$ Figure 4.2: Eigenvalues at $M_\infty^2 = 0.01$ and $Re = 100$ at $\eta = 0$

instead of four. These two eigenvalues are related to the energy equation and the incompressible Navier-Stokes equation respectively. For the latter equation only one eigenvalue may be expected because in this two-dimensional case one can rewrite it as a scalar equation in the stream function. We see that all eigenvalues are in the left half plane, so this indicates that the initial value problem is locally well-posed.

4.2 Stability

We now would like to investigate the behavior of solutions of the semi-discretized equations (3.2). If we linearize those equations in point (i, j) as:

$$\left(K \frac{d}{dt} + \Lambda\right) \phi_{ij} = 0 \quad (4.9)$$

with Λ the Jacobian of \mathbf{F} and K as in the linearized equations (4.1). Now we would like to locate the generalized eigenvalues of (4.9), so we can search for a method that has those eigenvalues within its stability region. We use therefore again Fourier analyses on the difference equation (4.9), replacing the ϕ with a Fourier component. And via the generalized eigenvalue problem we obtain the eigenvalues of the linearized discrete system. Figure 4.3 shows the eigenvalues with the same Reynolds number as obtained in the previous section and the mesh width is take $1/33$ in both directions. Now we know the system's eigenvalues, so we may choose from a wide range of integration methods. We will choose one of the *backward differentiation formulas* (BDF) [11], since their stability regions contain

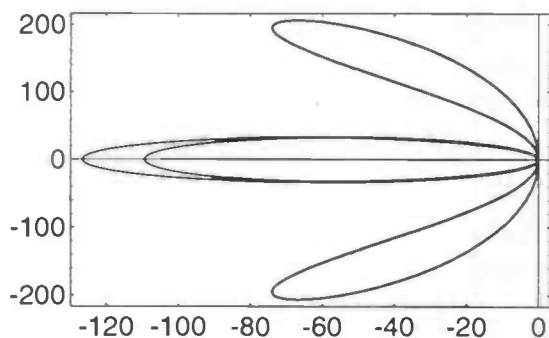


Figure 4.3: Eigenvalues at $M_\infty^2 = 0.1$ and $Re = 100$

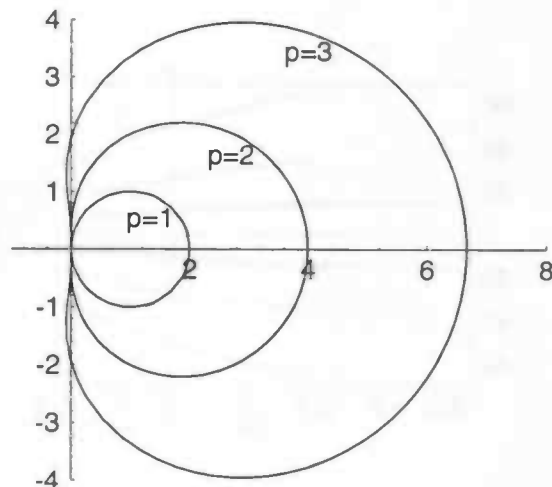


Figure 4.4: Stability regions of BDF-methods

most part of the left complex plane. Figure 4.4 shows the regions of stability for the BDFs of degree up to three. Note that the values shown in Figure 4.4 are in the $\delta t \lambda$ -plane, one should take that into account. For instance for sufficient small M_∞ and δt some eigenvalues could fall outside the stability regions. Considering this we will use the BDF of degree one or the Backward Euler method because its stability region surely contains the entire left plane. Hence (3.2) becomes

$$K(\varphi^{n+1}) \frac{1}{\delta t} (\varphi^{n+1} - \varphi^n) + \mathbf{F}(\varphi^{n+1}) = 0 \quad (4.10)$$

φ^n denotes φ at time $t = n\delta t$ and K a matrix .

In Chapter 3 we had chosen a mixed upwind/space-centered difference scheme. By using Taylor series we have first-order accuracy in space, concluding that the method is consistent. Together with the other investigations we have all the ingredients necessary for the application of the Equivalence Theorem. So based on local analysis of the problem, we have obtained a method that will converge.

Chapter 5

Implementation

5.1 Newton's method

In solving the system of equations (4.10) we make use of primitive variables u , v , p and T . Other quantities like averages, density and μ are functions φ of the primitive variables. We may write in a cell $\varphi = \varphi \circ \phi$, with ϕ the vector of the primitive variables. We now have as many equations as unknowns, so we effectively need to find a root of the vector $\mathbf{G}(\varphi \circ \phi) = 0$, which can be found by using the Newton-Raphson method:

$$\frac{\partial \mathbf{G}}{\partial \varphi} \cdot \frac{\partial \varphi}{\partial \phi}(\varphi \circ \phi_k) \Delta \phi = -\mathbf{G}(\varphi \circ \phi_k) \quad (5.1)$$

$$\phi_{k+1} = \phi_k + \Delta \phi \quad (5.2)$$

With $\frac{\partial \mathbf{G}}{\partial \varphi}$ the Jacobian matrix of \mathbf{G} . We now group the variables in each cell into a vector variable as $\mathbf{w} = [u_W, v_Z, p_C, T_C]^T$, as shown in Figure 5.1. So the Jacobian has a 9-block stencil; each block being a 4x4-matrix. The solver has an input only for a sparser 5-block stencil. That means that there is no place for the groups of variables in the corners. Therefore we have to modify the Jacobian matrix by introducing new functions $\tilde{\varphi}$ and $\tilde{\mu}$ for those groups of variables. In our case we approximate as follows:

$$\begin{aligned} v_5 &\approx \frac{1}{3}(v_N + v_Z + v_7) \\ v_6 &\approx \frac{1}{3}(v_N + v_Z + v_8) \\ u_2 &\approx \frac{1}{3}(u_W + u_O + u_1) \\ u_4 &\approx \frac{1}{3}(u_W + u_O + u_3) \\ \mu &\approx \mu_C \end{aligned}$$

If we introduce $\tilde{\mathbf{G}} = \mathbf{G}(\tilde{\varphi}, \tilde{\mu})$, the modified Jacobian matrix will be:

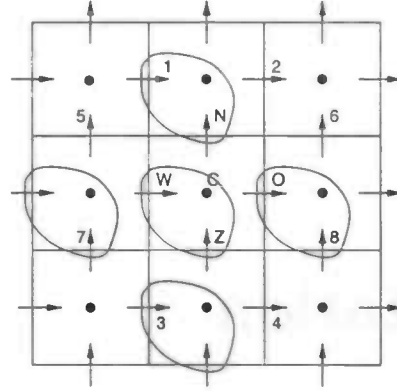


Figure 5.1: The five groups of variables

$$\frac{\partial \tilde{\mathbf{G}}}{\partial \tilde{\varphi}} = \frac{\partial \mathbf{G}}{\partial \varphi} \cdot \frac{\partial \tilde{\varphi}}{\partial \phi}(\varphi, \tilde{\mu}) \quad (5.3)$$

We let the $\tilde{\mu}$ unchanged in the Jacobian matrix, because μ does not vary much in the neighborhood of each cell if the Mach number is small ($\mu = 1 + O(\gamma M_\infty^2 T)$). For the same reason we use an approximated function for the derivative of $\tilde{\mu}$. The origin of the corner variables lies in the mixed derivative in the impulse equations and two derivatives in dissipation. What needs to be checked is whether the diagonal of the Jacobian matrix is weakened by those approximations. The derivatives in the energy equation (in the inner field) will be

$$u_y \doteq \frac{1}{k} \left[\frac{1}{3} (u_1 - u_3) \right]$$

$$v_x \doteq \frac{1}{h} \left[\frac{1}{3} (v_8 - v_7) \right]$$

and the derivatives in the impulse equations

$$u_{xy} \doteq \frac{1}{hk} \left[\frac{2}{3} u_O - \frac{1}{3} u_W + \frac{2}{3} u_3 \right]$$

$$v_{xy} \doteq \frac{1}{hk} \left[\frac{2}{3} v_N - \frac{1}{3} v_Z + \frac{2}{3} v_7 \right]$$

We can see that the approximations do not result in a weaker diagonal. A disadvantage is that we do not have the theoretical second order convergence as we would have without modification and in an exact computation.

5.2 The preconditioner

In order to improve the condition of the Jacobian matrix, we precondition the matrix with an incomplete LU -decomposition P of the Jacobian as done in [12].

This results in solving

$$P^{-1}J\phi = P^{-1}\mathbf{r} \tag{5.4}$$

with $J = P + R$. The construction of the LU -decomposition is basically a Gauss-elimination where elements of the matrix (the fill-in) are set to zero during the process of elimination. For more details see Reference [12]. The preconditioned system is solved by using the method BiCGstab(1) [13].

Chapter 6

Results

In this chapter a few comments are to be made on the settings of the used parameters in the system. Then the results will be discussed.

6.1 Reynolds number and artificial diffusion

When we study a convection-diffusion equation, we know that by using an upwind scheme for the convective part we have artificial diffusion. Thus, for a coarse grid large Reynolds numbers will resolve in solutions for relative smaller numbers. Comparing those solutions with solutions in the literature, Reynolds numbers up to 100 give appropriate results. In Figure 6.2 the solutions of two different grids are compared with [5] for $Re = 100$ and $M_\infty = 0$. All results in this chapter are obtained for $Re = 100$.

6.2 Time propagation to steady state

A way to compare solutions of the values of the different parameters is the investigation of their steady states. For Reynolds numbers up to 10000 there are known steady state solutions with an increasing number of eddies emerging when Reynolds is increasing and with a proper grid in order to capture those eddies. One has to think like 512x512 grid points, see References [5, 14] for examples. To determine those states we iterate as far in time when the maximum norm of \mathbf{F} (see Chapter 3) is decreased to *restol*. Or

$$\|\mathbf{F}(\phi^n)\|_\infty < \text{restol} \tag{6.1}$$

We iterate till the starting residue is less than 1E-5. Since the driven cavity with an impulsively started lid exhibits the typical behavior of an asymptotic approach to the steady state, the time step size may be increased for large t [6]. A way to determine the size of the time steps may be based on equal starting residue descent or another quantity like the propagation of the solution itself.

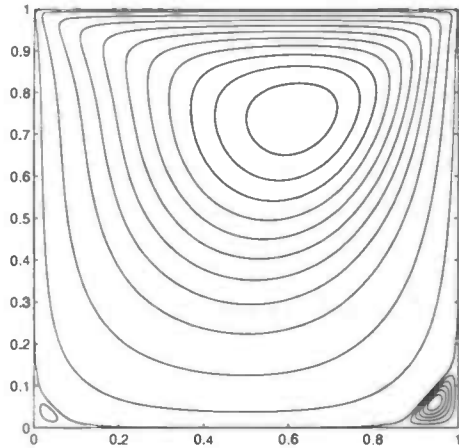


Figure 6.1: Stream lines

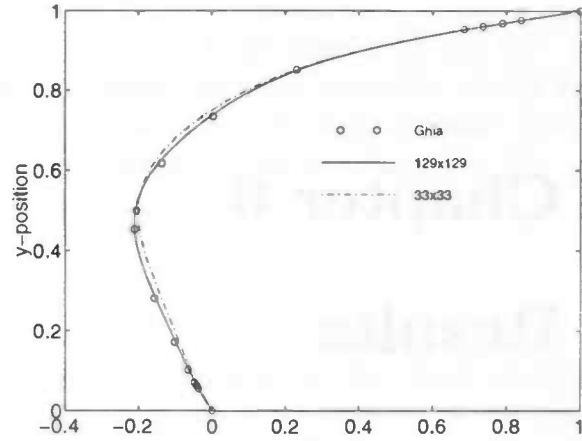


Figure 6.2: u -velocity at $x=0.5$

6.3 Time step

In all of our results we use the time solution of an impulsively started lid. The velocity of the lid is given by a step function $u|_{y=1} = U_\infty$ for $t \geq 0$ and $u|_{y=1} = 0$ for $t < 0$. At the initial stage of flow development as $t \downarrow 0$, a flow boundary layer forms along the lid away from the corners with the dimensionless thickness of $\delta \sim \sqrt{t/Re}$ [6]. Since the boundary layer thickness is extremely small for $t \downarrow 0$, it is difficult to resolve this boundary layer numerically unless an enormous number of grid points are employed. If we estimate the boundary layer thickness to be $\frac{1}{2}k$ which is the grid generated boundary layer between the lid and the immediately neighboring location of the u -velocity in the y -direction, then the time required for the growth of the boundary layer to the thickness is about $Re(\frac{1}{2}k)^2$. Generated solutions for the time far less that time may not be appropriate for physical interpretation. In Figure 6.3 the time development of the driven cavity with impulsively started lid is shown. One can see the building of the boundary layer in the first time steps.

6.4 Indefiniteness of the density

As mentioned before, the pressure and therefore the density is determined up to a constant when Mach number is taken zero. For Mach number greater than zero the pressure level is fixed via the continuity equation. As mentioned in Section 2.4 the time derivative of the density is indispensable when we would like to conserve mass in our cavity, but it is weakly described by the equation:

$$\gamma M_\infty^2 \frac{1}{\delta t} [\rho^{n+1} - \rho^n] + \mathbf{F}(\varphi) = \text{error} \quad (6.2)$$

The factor $\gamma M_\infty^2 \frac{1}{\delta t}$ will bound the error we may make in getting accurate solutions. As the limit $M_\infty = 0$ is taken there is no equation which describes the conservation

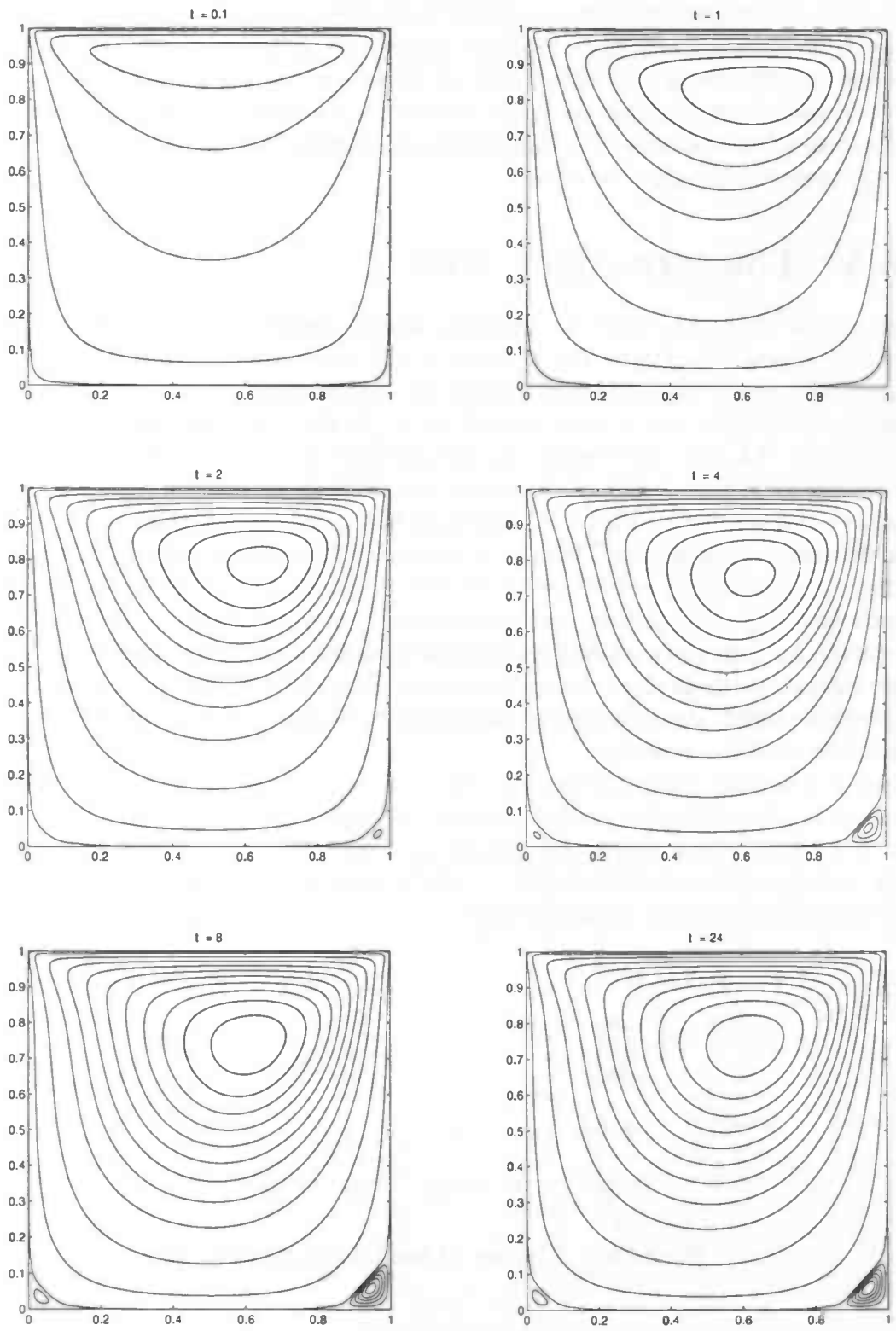


Figure 6.3: Time evolution

of mass. We might say that on a global scale $\frac{\gamma M_\infty^2}{\delta t} / error$ needs to be of order one, which gives a limitation on the time step size. A large time step like 10^{10} as taken in [15] hereby excluded. But we still have the extra condition (2.15) for the pressure which might help the system to maintain the right pressure level, also when Mach number is almost zero. In Chapter 7 we will discuss a way to implement the pressure condition.

6.5 The zero Mach limit

Now it is interesting how the pressure field is distributed as the Mach number tends to zero. In Figure 6.5 a detail of the pressure in the center of the cells along the upper edge is shown. Those are steady state solutions, with a Newton accuracy of $1E-6$ and a time step $\delta t = 1$. In the first case values for M_∞^2 are taken 0.8, 0.4, 0.1, $1E-7$ and 0. In the previous section the weak fixation of the pressure level was described. It stated that a high accuracy was needed to have mass conservation: in Figure 6.6 the same Mach number solutions are shown with a Newton accuracy of $1E-12$. As a matter of fact the accuracy predicted us a decoupling at about $M_\infty^2 = 1E-6$ in the first case and we can see in Figure 6.6 that only the $M_\infty^2 = 0$ solution has a questionable pressure level, compared with the others. An indication of that leap is leaking mass in the cavity, since the density is coupled to the pressure via the equation of state. In Table 6.1 the mass in the cavity is shown. And Figure 6.4 shows graphs of the total mass at different Mach numbers as time evolves.

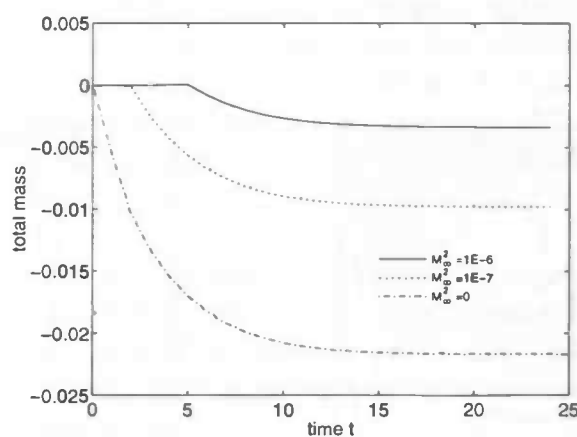


Figure 6.4: The loss of total mass, newtol=1E-6

Of course, by increasing the accuracy, mass conservation can be obtained, but it will cost runtime. We now have a reason to apply the extra pressure condition

M_∞^2	0.01	1E-3	1E-4	1E-5	1E-6	1E-7	0
Total mass	1.2E-7	3.4E-6	-1.1E-5	-9.9E-4	-0.0048	-0.0151	-0.0217

Table 6.1: Total mass in steady-state solution

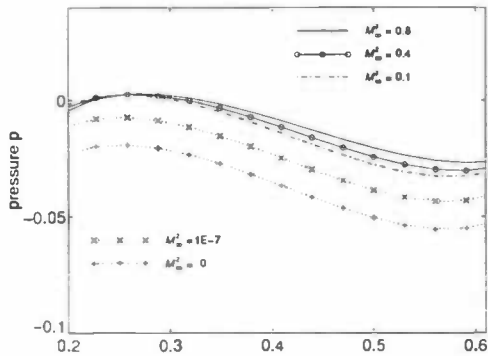


Figure 6.5: Pressure upper edge for newtol=1E-6

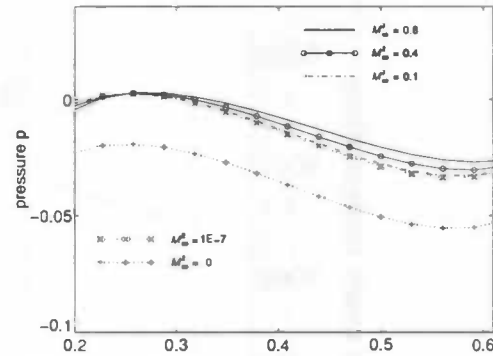


Figure 6.6: Pressure upper edge for newtol=1E-12

in the system of equations, what will be done in the next chapter.

In Figures 6.7 and 6.8 two other quantities are shown. Here we can see that the solutions converge smoothly as the Mach number is lowered. The accuracy is taken 1E-6.

Another matter is the performance in CPU-time as the Mach number is lowered. We use the amount of matrix multiplications as a first indication. A Mach sweep performance is made for a 1E-6 accuracy to obtain steady states on a 33x33, 17x17 and 9x9 grid and equal time steps of size 1. Figure 6.9 shows the results. It is clear that computational time increases when the Mach number is lowered. But

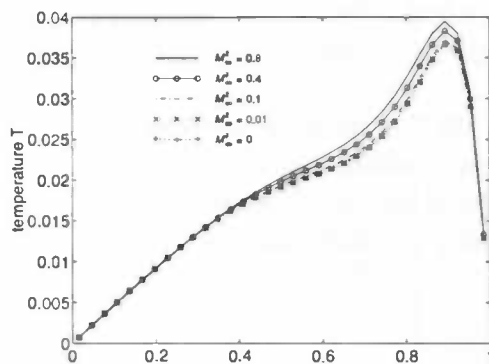


Figure 6.7: Temperature along $x = 0.5$

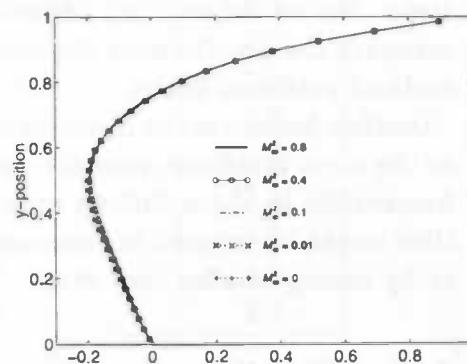


Figure 6.8: u -velocity along $x = 0.5$

at a certain point it drops.

In Table 6.2 information is given about the performance of the Newton's method

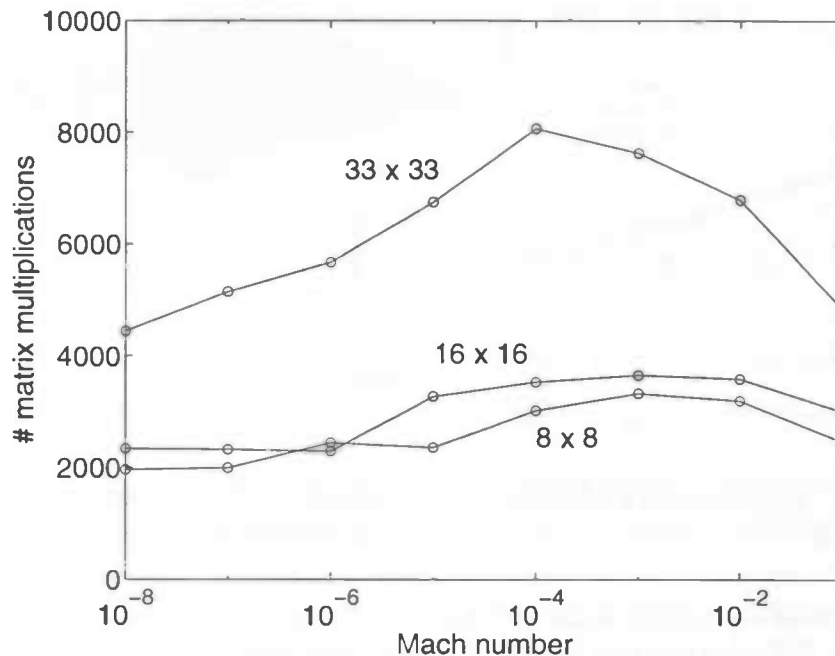


Figure 6.9: Number of matrix multiplications at different mesh configurations

we've used, including the amount of Newton iteration per time step and also the starting residuals are in the table. Further the amount of BiCGstab(8) per Newton step is given. The residual decreases slower when time evolves. We may use this to increase the time step size as mentioned in Section 6.3. From the numbers we see that our modified Newton method needs more iteration steps in the starting time steps. But as the solution becomes stationary less Newton steps are needed. If we compare the results with those of $M_{\infty}^2 = 0$ in Table 6.3 it is clear that Newton's method performs better.

Another feature is the increasing number of BiCGstab-steps per Newton iteration as the mesh is refined, possible due to the worse condition of the Jacobian as higher frequencies in the solutions may be represented by the system. The calculation time might be reduced in this case by decreasing the stop criterium in BiCGstab(1) or by taking smaller time steps.

6.6 Scaling performance

In this section the used scaling is tested on its properties. The derived new variables are expected to be of order one. In Figures 6.10 to 6.14 the quantities are shown

time	residue	#Newton steps	#BiCGstab(8) steps	av. BiCG steps
1	21.7800	9	3,3,2,3,3,2,8,8,3	3.9
2	0.8131	8	3,3,3,3,3,8,8,9	5.0
3	0.1327	7	3,3,2,3,8,9,3	4.4
4	0.5245E-1	7	3,3,3,3,9,10,3	4.9
5	0.2617E-1	5	3,3,3,3,4	3.2
6	0.1456E-1	4	3,4,3,3	3.3
7	0.8474E-1	4	4,3,3,3	3.3
8	0.5045E-2	4	4,3,3,3	3.3
12	0.6812E-2	3	4,3,3	3.3
16	0.1319E-3	3	3,4,4	3.7
20	0.3369E-4	2	3,4	3.5
24	0.8419E-5	2	3,3	3.0

Table 6.2: Solution statistics for $M_{\infty}^2 = 1E-6$

time	residue	#Newton steps	#BiCGstab(8) steps	av. BiCG steps
1	21.780	6	3,3,3,3,3,3	3.0
2	0.8132	6	3,3,3,3,3,3	3.0
3	0.1328	5	3,3,2,3,3	2.8
4	0.5245E-1	5	3,3,2,3,3	2.8
5	0.2617E-1	5	3,3,3,3,3	3.0
6	0.1456E-1	4	3,3,3,3	3.0
7	0.8474E-2	4	4,3,3,3	3.3
8	0.5045E-2	4	4,3,3,3	3.3
12	0.6813E-3	3	4,3,3	3.3
16	0.1716E-3	3	3,3,3	3.0
20	0.4331E-4	2	3,3	3.0
24	0.1075E-4	2	3,3	3.0
25	0.7581E-5	2	3,3	3.0

Table 6.3: Solution statistics for $M_{\infty}^2 = 0$

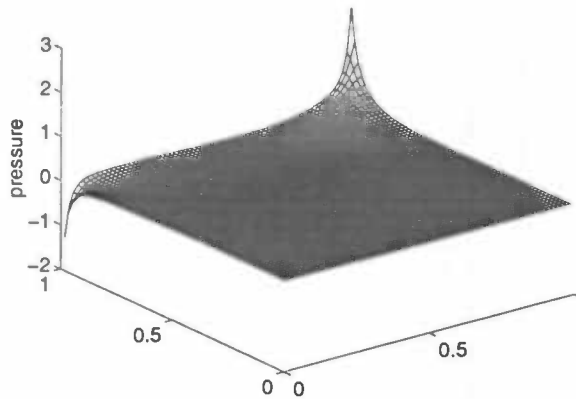


Figure 6.10: Pressure distribution

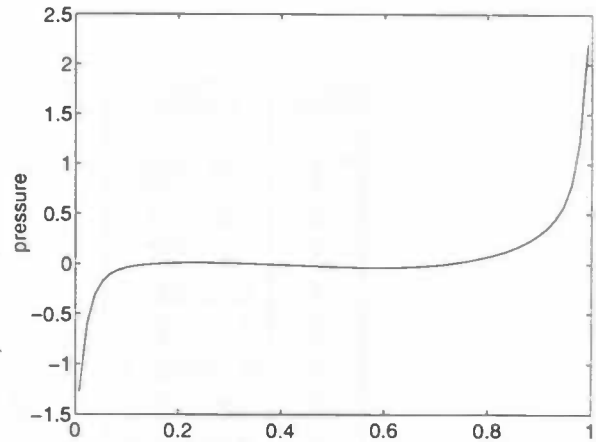


Figure 6.11: Pressure along the upper edge

grid	9x9	17x17	33x33	65x65	17x33	33x17	65x33
p_{min}	-0.1287	-0.2737	-0.5916	-1.2745	-0.3659	-0.3699	-0.7939
p_{max}	0.4468	0.7979	1.3208	2.2096	0.8982	1.0465	1.6862
T_{min}	0.0002	0.0001	0	0	0.0000	0.0001	0.0000
T_{max}	0.0570	0.0657	0.0736	0.0791	0.0703	0.0726	0.0770
ρ_{min}	-0.1664	-0.3176	-0.6393	-1.3216	-0.4197	-0.4016	-0.8266
ρ_{max}	0.3867	0.7264	1.2406	2.1197	0.8198	0.9908	1.6275

Table 6.4: Minima and maxima on different grids

for a 65x65 grid for Mach number $M_\infty^2 = 0.1$. We can see clearly that the driven cavity has two singularities in the top left and right corner. Figure 6.16 focusses on the left one for different grid configurations.

As the grid is refined the singularities become dominant. On coarse grids the minimum and maximum values are of order 1. It is not so strange this is happening if we look at the behavior of the velocities in those corners. In Figure 6.15 we see a detail of Figure 6.1. The strong turn in the stream lines causes large velocity derivatives in the impulse equations. In Table 6.4 the extremes of the quantities are shown. The temperature has low extreme values. If we look at the distribution of the temperature on the edge we see a smooth curve except in the corners. This is caused by the $O(h, k)$ approximation of the pressure gradient on the edge appearing in the upwind scheme in the energy equation.

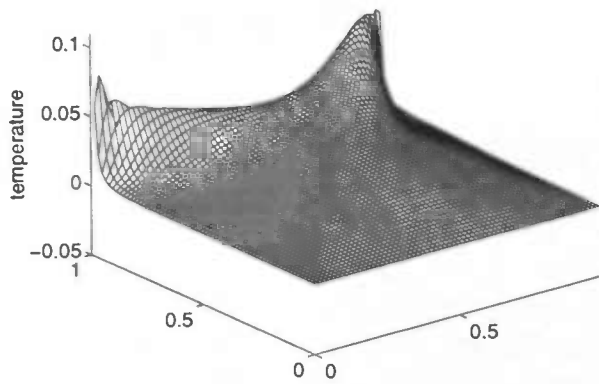


Figure 6.12: Temperature distribution

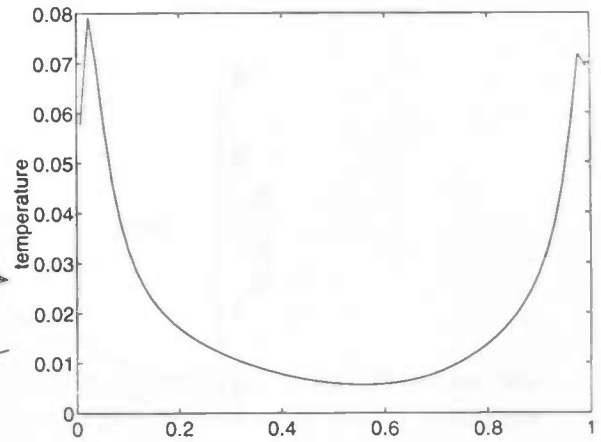


Figure 6.13: Temperature along the upper edge

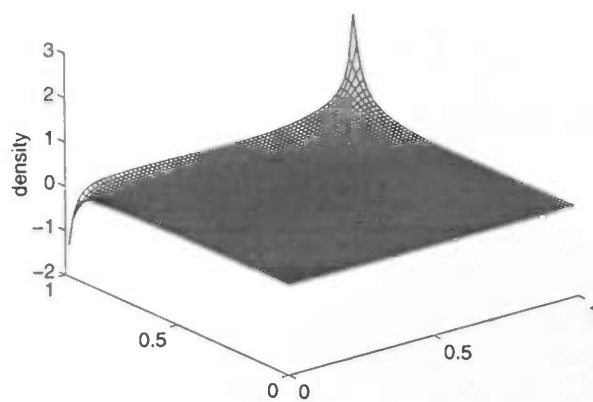


Figure 6.14: Density distribution

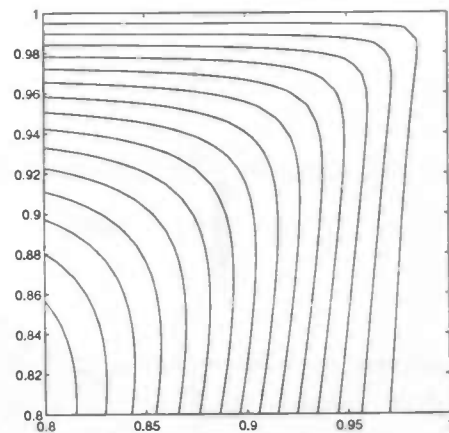


Figure 6.15: Streamlines in top right corner

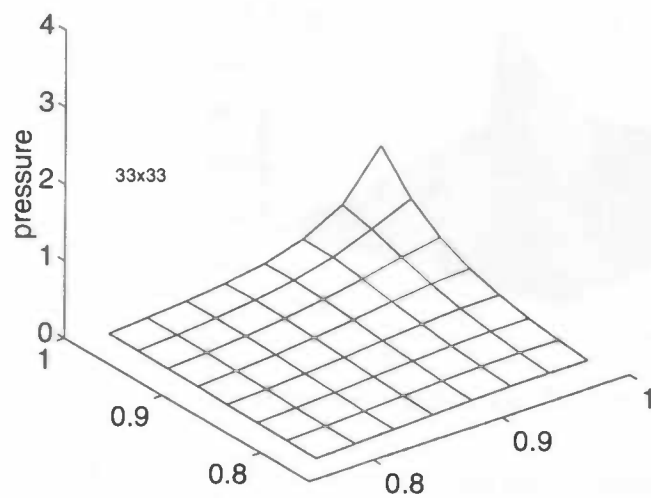


Figure 6.16: Detail of pressure on 33x33 grid

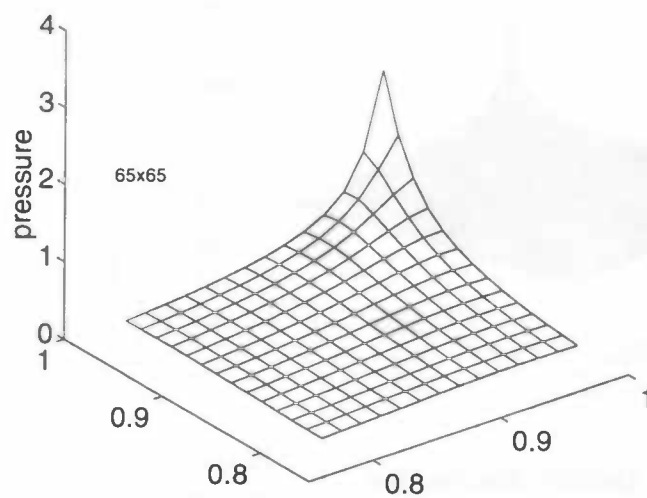


Figure 6.17: Detail of pressure on 65x65 grid

Chapter 7

Mass conservation

There is loss of mass in our cavity due to stopping criteria and roundoff errors (see Section 6.5). If we investigate the differences in the solutions of 'Mach is almost zero' and the others, it is clear that the pressure field shows the relative largest difference. More precise, it differs *approximately* a constant value. The idea is to correct the density with a constant $\Delta\rho$ and via the equation of state we derive the pressure correction.

Assume we differ $m = M - \sum \rho_{ij}V_{ij}$, with M the total mass on $t = 0$, then a density correction as above is applied, i.e., $\Delta\rho = m / \sum V_{kl}$. Using the equation of state

$$\begin{array}{rcl} p' & = & (\gamma M_\infty^2 T + 1) \rho' + T \\ p & = & (\gamma M_\infty^2 T + 1) \rho + T \\ \hline \Delta p & = & (\gamma M_\infty^2 T + 1) \Delta\rho \end{array} \quad (7.1)$$

we obtain mass conservation if

$$\Delta p_{ij} = m(\gamma M_\infty^2 T_{ij} + 1) / \sum V_{kl} \quad (7.2)$$

In our case we have (the dimensionless) total mass of 0, cells of equal size and a total volume of 1, so we may write:

$$\Delta p_{ij} = \frac{-(\gamma M_\infty^2 T_{ij} + 1)}{\#\text{cells}} \sum \rho_{kl} \quad (7.3)$$

and we see that for $M_\infty = 0$ the entire pressure field is corrected with a constant. In Figure 7.1 the same tests are performed as in the previous chapter with our pressure correction. Now the results are more useful for the investigation of the limit $M_\infty \rightarrow 0$. From the tests we see that the solution of $M_\infty = 0$ is of the same level as the other solutions. The solutions are in agreement with those in Figures 6.5 and 6.6.

If we compare the amount of matrix multiplications of the calculation with those without the pressure correction we see no relevant differences between them. In Figure 7.2 the numbers are shown.

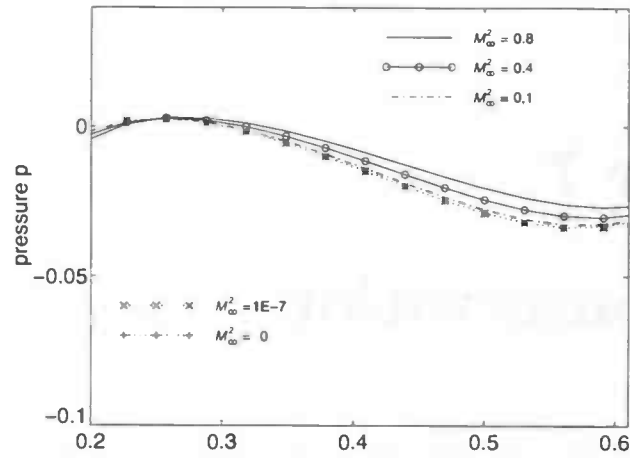


Figure 7.1: Pressure upper edge with correction with newtol=1E-6

Remark: Another way of imposing mass conservation is by augmenting the equations with the equation

$$\sum \rho_{ij} V_{ij} = 0 \quad (7.4)$$

or in the case of constant cell volume $\sum \rho_{ij} = 0$. Herewith the set of equations is over determined but still solvable, for $M_\infty > 0$. We have not implement this variant as the earlier proposed way already performed well.

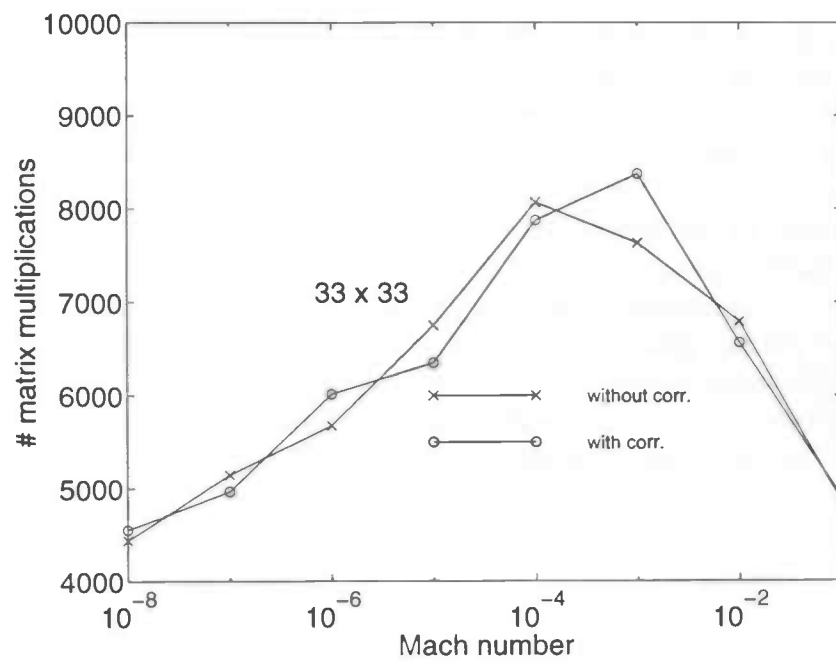


Figure 7.2: Number of matrix multiplication with and without correction

Chapter 8

Pushing the method to its limits

In the process of investigating the limits of our method, several problems came along. We have already seen good results in letting Mach number to zero. Even though we did our calculation in the subsonic region we would like to see how the method performs in supersonic flows: $M_\infty \rightarrow \infty$. Based on the assumption taken while modifying Newton's method (Section 5.1) it is clear we could expect decreasing convergence properties. It is also interesting to monitor the factor $\gamma M_\infty^2 \rho + 1$ which figures in every equation. What we know is that this factor has to be non-negative, because it is the original scaled density ρ/ρ_∞ . It is also known that the driven cavity has two singularities and especially the left top corners may cause negative values of the density, which is not correct physically. If we look at moderate Mach number, the ones we have chosen in our investigation, no negative values appear. In Figure 8.1 the factor is shown. But if we increase the Mach

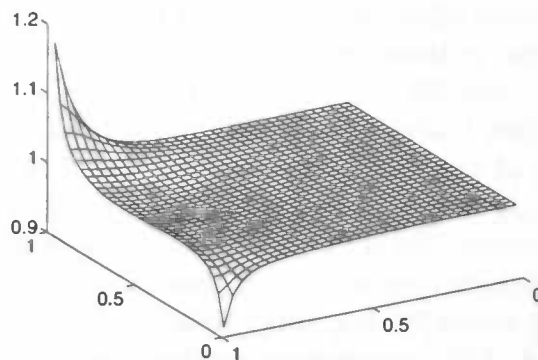


Figure 8.1: Factor $\gamma M_\infty^2 \rho + 1$ for $M_\infty^2 = 0.1$

number, the factor becomes negative (see Figure 8.2). What has happened is odd/even decoupling in the continuity equation. Let say that the u -velocity near

the upper edge nearly constant, $u \approx u_0$, then the continuity equation becomes $\frac{1}{\delta t}[\rho_C^{n+1} - \rho_C^n] + u_0[\rho_O - \rho_W] = \text{error}/\gamma M_\infty^2$ and since ρ_O and ρ_W are functions in the averages of p and T it calls for the odd/even decoupling. In Figure 8.4 we see the pressure distribution at the edge for $M_\infty^2 = 10$ during iteration on $t = 0.3$, and the next time step Newton's method does not converge. If we look at the density factor as above, we see negative values. This causes a non-physical situation and is doomed to fail as more time steps are calculated. It is clear that the central discretization is the trouble maker. What is an alternative? We would like to have smooth solutions and numerical mass conservation. A way to achieve that is an upwind treatment of the density, in which the direction is based on the velocities in the centers of the cell edges:

$$\frac{\partial}{\partial x}(\gamma M_\infty^2 \rho + 1)u|_C \doteq \frac{1}{h} \left[\begin{array}{l} (\gamma M_\infty^2 \rho_C + 1)u_O \quad \text{if } u_O > 0 \\ (\gamma M_\infty^2 \rho_{CO} + 1)u_O \quad \text{if } u_O < 0 \\ (\gamma M_\infty^2 \rho_{CW} + 1)u_W \quad \text{if } u_W > 0 \\ (\gamma M_\infty^2 \rho_C + 1)u_W \quad \text{if } u_W < 0 \end{array} \right] \quad (8.1)$$

or $(\frac{1}{\delta t}I + U)\bar{\rho}^{n+1} = \frac{1}{\delta t}\bar{\rho}^n$ where U is a matrix filled with values of velocities and $\bar{\rho}$ a vector of $\gamma M_\infty^2 \rho + 1$ values. One can prove that for all time step sizes the matrix $\frac{1}{\delta t}I + U$ is diagonal dominant with respect to its columns and it has positive elements on the diagonal and negative values outside the diagonal, hence it is an M -matrix. Consequently it is monotone and therefore its inverse matrix is positive. Hence, if $\bar{\rho}^n > 0$ then $\bar{\rho}^{n+1} > 0$. Figure 8.3 shows the factor in the center of the cell on the edge and we see that the values are non-negative and there are no wiggles in the solution. Further results show bounded solutions for large Mach numbers. And for all Mach numbers a slower convergence in Newton's method than the rate with the former discretization.

Another problem rises when small Reynolds numbers ($Re < 5$) are taken. Newton's method diverges in those cases when Mach number is unequal to zero. (for example $M_\infty^2 = 0.1$ and $Re = 1$). Again, by taking small time steps Newton's method converges, but badly. Closer investigation shows a bad convergence rate in the singularities of the driven cavity. The first step of our Newton method gives a first correction that causes again undesired negative values of $\bar{\rho}$. Another possibility to circumvent this is to force the method to keep the right sign for $\bar{\rho}$. There are various ways to impose that. If small Mach numbers are taken, than we approximate $\bar{\rho}$ with a zero Mach number solution, but it shows a bad convergence of Newton's method. This convergence problem could not be solved satisfactorily within the project and is left for the future.

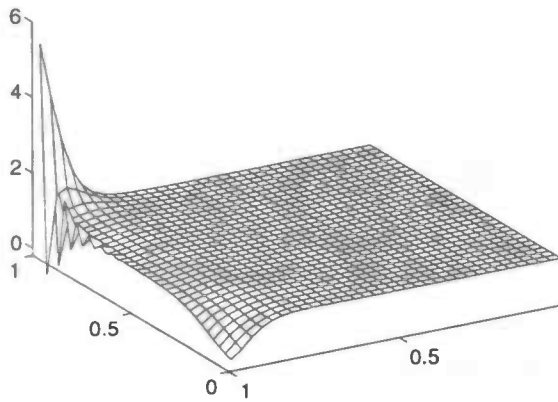


Figure 8.2: Factor $\gamma M_\infty^2 \rho + 1$ with central discretization

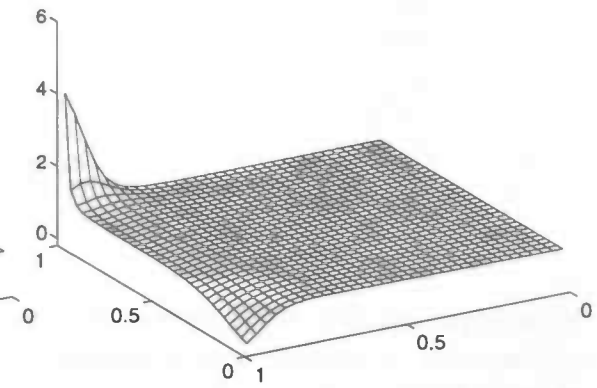


Figure 8.3: Factor with upwind discretization

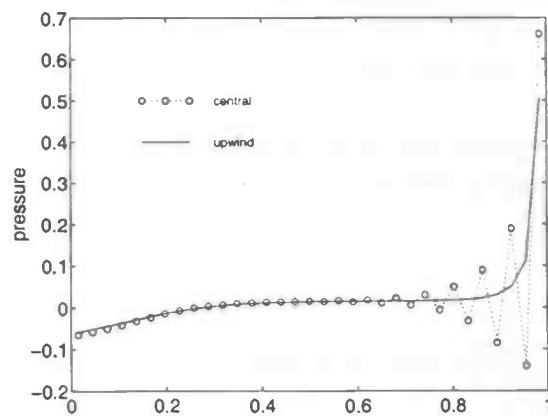


Figure 8.4: Pressure distribution on the edge for $M_\infty^2 = 10$



Chapter 9

Concluding remarks

We succeeded in making one method for both compressible and incompressible flow problems. The essential point in developing such a method is the scaling. The present scaling is chosen in a way that (i) the influence of roundoff error is eliminated at low Mach numbers and (ii) the scaled variables have about the same magnitude. The latter prevents under- and overflow.

Numerical experiments on the square driven cavity showed that

1. the zero Mach limit was performed smoothly,
2. the zero Mach limit solutions are in good agreement with those obtained by solvers for the incompressible flow found in the literature.

The continuity equation after scaling give rise to an indeterminacy of the scaled density in the zero Mach case. This is an immediate consequence of the indeterminacy of the pressure in the incompressible flow. This causes already some loss of mass for low Mach numbers as the equations are not satisfied exactly due to stopping criteria and roundoff errors.

Moreover it results in a wrong computation of the energy. We repaired this by requiring that the total scaled mass is also conserved at zero Mach (as it is for all Mach numbers not equal to zero).

This yields that

1. the pressure is completely determined at zero Mach,
2. the solution at zero Mach can be used to compute the solution at small Mach numbers.

Numerical trouble occurred for high Mach numbers and low Reynolds numbers. Wiggles emerged from one end of the driven lid resulting in an unphysical negative density which in turn caused a numerical blow up. This problem was cured by

using an upwind scheme in the continuity equation. Herewith one can show that the density remains positive.

the computing time of the new method behaves in general quite smooth as a function of the Mach number. Of course it is strongly dependent on the stop tolerance in the Newton method.

For the future we suggest to derive a conservative alternative to the one presented here. Conservative forms are more commonly applied in fluid flows and are necessary for a proper handling of (near) discontinuities in the flow (e.g. shocks).

Though the driven cavity is a rather hard problem it is also important to study this method for other problems.

Chapter 10

The code

The main program is briefly as follows:

```
5 CONTINUE
10 CONTINUE
  CALL filljac
  CALL fillrhs
  CALL prec
  CALL bicgstabl
  IF (newcorr.GE.newtol) GOTO 10
  CALL zeromass
  IF (startres.GE.restol) GOTO 5
```

In the inner loop is a Newton iteration process. In every step the Jacobian and the right-hand side will be filled with the solution of the previous time step and the same solution as an initial guess for the Newton's method. Next a preconditioner for the linear system is derived. The preconditioned system will be solved in BiCGStab(*l*). This loop ends when the correction is small enough. After that pressure correction is employed.

The outer loop is the time iteration. This loop will be terminated when the starting residual or the norm of the right-hand side at the beginning of the Newton iteration process is less than a certain value. In a short notation it reads:

$$\|\Delta\phi_{k+1}^{n+1} - \Delta\phi_k^{n+1}\|_{\infty} \leq \text{newtol}$$

$$\|\mathbf{F}(\varphi^n)\|_{\infty} \leq \text{restol}$$

where *k* denotes the Newton step counter and *n* the time step counter.

The following routines are used:

filljac, fillrhs

The filling of the Jacobian matrix *J* and the right hand side vector *r*. The matrix will be stored in 5 arrays *A*, *B*, *C*, *D* and *E* of size $4(N_x + 1)(N_y + 1) \times 4$ and vector

\mathbf{r} has a length of $4(Nx + 1)(Ny + 1)$.

The construction of the preconditioner P . This is stored in the arrays a_1, a_2, \dots, a_9 of size $4M$, with M the amount of levels that are used to construct the preconditioner.

bicgstabl

This routine solves the system $P^{-1}J\phi = P^{-1}\mathbf{r}$ using the iterative method BiCGstab(l). Its stop criterium is given by $\|P^{-1}(\mathbf{r} - J\phi_k)\|_2 \leq tol\|P^{-1}(\mathbf{r} - J\phi_0)\|_2$, saying that the residue has to be reduced to a factor tol .

zeromass

This routine calculates the the total mass in the discrete system and correct the pressure field to obtain zero mass.

Bibliography

- [1] Hans Thoman Jörn Sesterhenn, Bernard Müller. Flux-vector splitting for compressible low Mach number flow. *Computers fluids*, 22(4/5):441-451, 1993.
- [2] R. Klein. Semi-implicit extension of a Godunov-type scheme based on low Mach number asymptotics I: one-dimensional flow. *J. of Comput. Phys.*, 121:213-237, 1995.
- [3] S.J. Shamroth W.R. Briley, H. McDonald. A low Mach number Euler formulation and application to time-iterative LBI schemes. *AIAA J.*, 21(10):1467-1469, 1983.
- [4] Frank Mangrem White. *Viscous fluid flow*. McCraw-Hill Book Company, USA, 1974.
- [5] L.T. Shin U. Ghia, K.N. Ghia. High-Re solutions for incompressible flow using the Navier-Stokes equations and a multi-grid method. *J. of Comput. Phys.*, 48:387-411, 1982.
- [6] John W. Goodrich W.Y. Soh. Unsteady solutions of incompressible Navier-Stokes equations. *J. of Comput. Phys.*, 79:113-134, 1988.
- [7] A.E.P. Veldman R. Verstappen, J.G. Wissink. Direct numerical simulations of driven cavity flows. *Appl. Sci. Res.*, 51, 1993.
- [8] Pieter Wesseling Hester Bijl. A method for the numerical solution of the almost incompressible Euler equations. 1996. Report 96-37.
- [9] A.E.P. Veldman. Numerieke stromingsleer. *Lecture Notes, University of Groningen*, 1994.
- [10] E.F.F. Botta. Eindige differentie methoden. *Lecture Notes, University of Groningen*, 1992.
- [11] Wilhard L. Miranker. *Numerical methods for stiff equations (and singular perturbation problems)*. D. Reidel Publishing Company, Dordrecht, 1981.

- [12] G. Tiesinga. Block preconditioning BiCGstab(2) for solving the Navier-Stokes equation. *Zeitschrift für angewandte Mathematik und Mechanik (ZAMM)*, 76, 1996.
- [13] Diederik R. Fokkema Gerard L.G. Sleijpen. BiCGstab(1) for linear equations involving unsymmetric matrices with complex spectrum. Technical Report 772, University Utrecht, dep. of math., March 1993.
- [14] L.B. Zhang Ch.N. Bruneau, C. Jouron. Multigrid solvers for steady state Navier-Stokes equations in a driven cavity. *Lecture Notes in physics*, 323, 1988.
- [15] G.E. Schneider S.M.H. Karimian. Pressure-based control-volume finite element method for flow at all speeds. *AIAA J.*, 33(9):1611–1618, 1995.